Biosensors and Bioelectronics 52 (2014) 337–344

Contents lists available at ScienceDirect

Biosensors and Bioelectronics

journal homepage: www.elsevier.com/locate/bios

Improved detection limits of protein optical fiber biosensors coated with gold nanoparticles

Sandrine Lepinay [a,b,*], Alyssa Staff [b], Anatoli Ianoul [b], Jacques Albert [b]

[a] Department of Electronics, Carleton University, 1125 Colonel By Drive, Ottawa, Canada K1S 5B6
[b] Department of Chemistry, Carleton University, 1125 Colonel By Drive, Ottawa, Canada K1S 5B6

ARTICLE INFO

Article history:
Received 24 July 2013
Received in revised form
26 August 2013
Accepted 27 August 2013
Available online 14 September 2013

Keywords:
Avidin-biotin complex
Biosensors
Gold nanocages
Gold nanospheres
Tilted fiber Bragg grating

ABSTRACT

The study presented herein investigates a novel arrangement of fiber-optic biosensors based on a tilted fiber Bragg grating (TFBG) coated with noble metal nanoparticles, either gold nanocages (AuNC) or gold nanospheres (AuNS). The biosensors constructed for this study demonstrated increased specificity and lowered detection limits for the target protein than a reference sensor without gold nanoparticles. The sensing film was fabricated by a series of thin-film and monolayer depositions to attach the gold nanoparticles to the surface of the TFBG using only covalent bonds. Though the gold nanoparticle integration had not yet been optimized for the most efficient coverage with minimum number of nanoparticles, binding AuNS and AuNC to the TFBG biosensor decreased the minimum detected target concentrations from 90 nM for the reference sensor, to 11 pM and 8 pM respectively. This improvement of minimum detection is the result of a reduced non-specific absorption onto the gold nanoparticles (by functionalization of the external surface of the gold nanoparticles), and of an optical field enhancement due to coupling between the photonic modes of the optical fiber and the localized surface plasmon resonances (LSPR) of the gold nanoparticles. This coupling also increased the sensitivity of the TFBG biosensor to changes in its local environment. The dissociation constant (K_d) of the target protein was also characterized with our sensing platform and found to be in good agreement with that of previous studies.

1. Introduction

Interest in biosensors extends not only to research but also to industry applications where detection, diagnosis and determination of biomolecules are high priorities. Some such industry fields include food- and water-quality control, security, and health, all of which have a continuously increasing demand for biosensors. The current challenge is to design simple, inexpensive, accurate, sensitive and reliable biosensor platforms. In response to this, many devices and methods have been developed to detect binding events, though optical measurement is the most widely used of the transduction methods. Among optical-based biosensors, optical fibers are new, tiny, flexible platforms that are being used with increasing frequency as biosensor transducers. Optical fibers are able to make quick and sensitive responses, and can be employed as an intrinsic or extrinsic biosensor (Nguyen et al., 2012). The biosensors presented in this work were intrinsic-type, label-free biosensors, utilizing a single-mode tilted fiber Bragg grating (TFBG). This optical fiber biosensor platform was classified as an evanescent wave sensor and combined various technologies to create a simple and robust platform that has been successfully applied to a wide range of interactions (Maguis et al., 2008). Recently, the Albert group has demonstrated that the efficiency of such TFBG sensors can be further improved by coating the fiber with a thin metallic layer, thus allowing the excitation of surface plasmon polaritons (Shevchenko et al., 2011). By the same principle, the Albert group also showed that TFBG are able to excite localized surface plasmon resonances (LSPR) in nanoscale particles (Bialiayeu et al., 2012). The unique optical property of supporting LSPR have made noble metal nanoparticles the subject of much research interest, and they are also of key importance in various studies of biological applications, including bioactive colloidal crystals (Gosecka et al., 2011), immunodiagnostic assays (Bousalem et al., 2005), chemical sensors (Gehan et al., 2010; Kaewsaneha et al., 2013), biosensors (Bedford et al., 2012; Bernand-Mantel et al., 2010), plasmonic nanostructures (Fang and Zhu, 2013), and hybrid nanocomposites (Rozenberg and Tenne, 2008; Spitalsky et al., 2010; Zou et al., 2008). This popularity and diversity stems from the fact that LSPR, compared to surface plasmon resonances (SPR), are much more localized, allowing for probing processes at the platform interface with spatial sensitivities well within the nanometer scale (Anker et al., 2008; Mayer and Hafner, 2011; Piliarik et al., 2012).

The majority of nanoparticle-enhanced SPR studies reported to-date have been focused on the use of DNA-functionalized gold nanoparticles (typically 10–15 nm in diameter), because of the

* Corresponding author at: Department of Electronics, Carleton University, 1125 Colonel By Drive, Ottawa, Canada K1S 5B6. Tel.: +1 613 520 1636.
E-mail address: sandrine.lepinay@carleton.ca (S. Lepinay).

0956-5663/$ - see front matter © 2013 Elsevier B.V. All rights reserved.
http://dx.doi.org/10.1016/j.bios.2013.08.058

well-established procedures for the preparation of DNA conjugates on planar gold surfaces (Gosecka et al., 2011; Hayashida et al., 2005). However, for planar detection of SPR, there are currently very few reports concerning larger nanoparticles sizes or non-spherical particles for the detection of proteins or nucleic acids (Sendroiu et al., 2009; Sim et al., 2010; Yu and Irudayaraj, 2007). The most complete study of this line of investigation to-date compared different nanoparticle shapes and sizes as part of a sandwich assay in combination with a gold SPR chip for the detection of thrombin to demonstrate that attomolar concentrations can be detected by this technique (Kwon et al., 2012). Branching from the utilization of LSPR with a gold planar surface, other studies using silica nanoparticles have been reported (Lin et al., 2009; Lin et al., 2010; Patolsky et al., 2006). For instance, Li et al. (2013) showed that transistor biosensors using silicon nanowires for the detection of protein could reach detection limits on the order of femtomolar concentrations. However, the study and work presented herein is the first known report of coupling TFBG and noble metal nanoparticles for the fabrication of biosensors.

These experiments were carried out using an unmodified and inexpensive standard telecommunication single-mode fiber. From the optics point of view, it is well known that a single-mode fiber's transmission power loss is less than 4%/km (Corning, 2010), making optical fibers well suited for remote operation over large distances (up to several kilometers). Moreover, the flexibility of optical fibers allows for a very robust sensor that is also simple to manufacture and to measure, using widely available instrumentation developed by the telecommunications industry. A TFBG transducer also offers very important advantages for sensor platforms in its temperature insensitivity and the preservation of the fiber's structural integrity under stressful environments (Albert et al., 2013; Chan et al., 2007).

Recent work prior to this study had demonstrated that silver nanowires can be used to significantly amplify the sensitivity of the TFBG sensor by introducing large and distinct anisotropy with respect to optical transmission (Bialiayeu et al., 2012). With this amplification of sensitivity in mind, it was decided to transfer this technique to a biosensor application. Two biosensors using gold nanoparticles (nanospheres and nanocages respectively) were studied and compared to a reference biosensor without nanoparticles. The amplification performance of the gold nanoparticles with respect to the enhancement of the LSPR was monitored by the detection of a protein. The goal of this study is to determine the influence of the nanoparticles' shape or surface area in contact with the biosensor platform on the LSPR properties, as evidenced by spectral shifts of the TFBG response due to LSPR changes. The gold nanospheres (AuNS) obtained for this study had a maximal absorbance in colloidal solution at a wavelength of 530 nm, whereas the LSPR of the gold nanocages (AuNC) in colloidal solution is in the visible and near-infrared (vis–NIR) range depending on the size and porosity of the nanocages (Skrabalak et al., 2008). The nanocages also provide a larger contact area as binding can occur on the inside surfaces. The TFBG spectral region of interest ranges from 1520 to 1620 nm, because of the high quality factor resonances that can be generated at those wavelengths. Gold nanoparticles were of interest for this range because of their LSPR sensitivity within the near-infrared (NIR) and infrared (IR) ranges of the electromagnetic spectrum when arranged in supported nanostructures, including when deposited on optical fibers, as described in this work. In previous work it was determined that the propagating modes of optical fibers are strongly perturbed within the region of interest by very sparse coatings of metallic nanoparticles (Bialiayeu et al., 2012; Shao et al., 2011; Zhou et al., 2013). This perturbation is caused by coupling between the resonance of the fiber cladding-mode and the localized plasmonic resonances of the nanoparticle coatings, including collective resonance modes that occur at longer wavelengths. The result of such coupling is the increase of the effective refractive index of the fiber's cladding-modes thereby causing measurable wavelength shifts of the grating resonances. The effective refractive index of an optical fiber is typically altered by varying the type and nature of the fiber's cladding (Albert et al., 2013), though in the work presented here, the cladding is instead modified by the interaction of gold nanoparticles.

Molecular recognition is the main criterion of general biosensing, thus the essential component of an effective biosensor is the ability of a specific molecular recognition probe to selectively target the desired analyte. For this study, biotin was chosen as the target molecule. The biotin molecules were to be bound to avidin molecules that had been covalently attached to the gold nanoparticles, which were in turn immobilized on the TFBG surface. Biotin/avidin combination chemistry has been used extensively as a model in protein sensing, primarily because of the strong attraction between the two ($K_d = 10^{-15}$ mol/L). The complex biotin/avidin has been applied successfully as molecular recognition probes for a variety of sensor techniques, including prism-based SPR and surface-enhanced Raman spectroscopy (Fu et al., 2013), as well as nanoscale field-effect transistors (Li et al., 2013). Utilizing the advantages of this well-known complex with its strongly recognizable affinity and signature in combination with the easily-obtained and durable platform of a TFBG, determining the effectiveness of a biosensor comprised of gold nanoparticles on the surface of a single-mode fiber platform was the key interest in this study. The experimental results indicated that the nanoparticle-incorporated biosensors can be used for the real-time monitoring of both the self-assembly of the sensing film on the TFBG surface, as well as for the detection of protein at various concentrations in aqueous solutions. The dissociation constant (K_d) of the target biotin bound to the avidin biosensor surface was also determined and was found to be comparable to that found in other biotin/avidin complex studies.

2. Materials and methods

2.1. The TFBG basic sensor

The optical fiber sensor used was made up of a standard single-mode optical fiber (Corning SMF-28) with a TFBG inscribed in the fiber's core. The TFBG was manufactured using intense ultraviolet light at 193 nm from a pulsed laser incident source on a phase mask, inscribing the grating in the fiber's core. The grating's planes were inscribed with a tilt of 10° relative to the normal axis of the fiber (as seen in Fig. 1). This angle allowed the sensor to operate in aqueous solutions with refractive indices between 1.31 and 1.34 RIU. After the grating was inscribed, a thin gold mirror was formed by electroless deposition on the downstream end of the Bragg grating. This technique is based on the reduction of metallic ions from a solution to a solid surface without electrical potential (Bialiayeu et al., 2011; Hrapovic et al., 2003). The interest of depositing a mirror at the end of the fiber is in that it allows a convenient and easy use of the sensor since it can be simply dipped directly into the testing and sampling solutions. In a TFBG sensor, coupling between the forward-propagating core-modes and the counter-propagating cladding-modes occurs, yielding a familiar transmission spectrum (inset in Fig. 1(B)). The molecular recognition event is measured through changes in the spectral transmission response of the TFBG (as described in Section 2.4 below).

2.2. Synthesis of gold nanocages

Gold nanocages were synthesized by a two-step process involving the synthesis of silver nanocubes followed by the galvanic

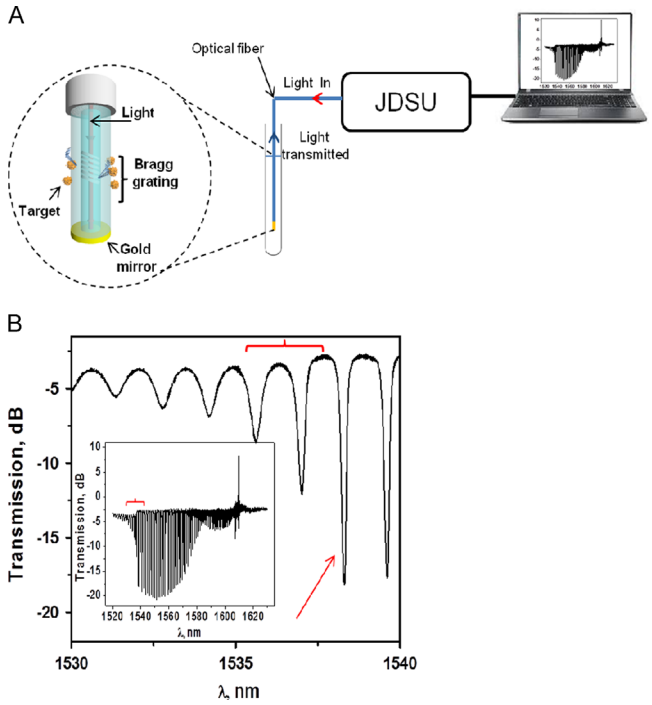

Fig. 1. (A) TFBG sensor setup with a reflective mirror; (B) inset shows a typical spectrum of the transmitted light after reflection in the gold mirror with the cut-off area indicated by the red bracket. The red arrow shows the wavelength of 1538 nm under observation throughout the study. (For interpretation of the references to color in this figure legend, the reader is referred to the web version of this article.)

displacement of silver with gold to form the gold nanocages. All non-water reagents and solvents were purchased from Sigma-Aldrich Co.

The silver nanocubes were synthesized using a basic polyol method well known in literature (Mahmoud et al., 2011). 35 mL of ethylene glycol was heated to 150 °C and stirred in a round-bottomed flask submerged in an oil bath for 1 h. Solutions of poly (vinylpyrrolidone) (PVP, 55,000 MW), sodium sulfide (Na_2S), and silver nitrate ($AgNO_3$) were prepared in ethylene glycol to concentrations of 80 mg mL^{-1}, 3 mM, and 282 mM respectively. 5 mL of the prepared PVP solution was added to the hot ethylene glycol and stirred for 10 min. 400 μL of the Na_2S solution was then added and stirred for 5 min. 2.5 mL of the $AgNO_3$ solution was then added at a rate of approximately 1 mL min^{-1}, with continued heating and stirring. The color change of the solution from clear and colorless to opaque greenish-grey was a good indication of the progression of the reaction. The shape and size of the synthesized particles was monitored by ultraviolet–visible (UV–vis) spectroscopy by extracting a small aliquot of the reaction solution and diluting it in ethanol. The reaction was quenched by placing the reaction flask into an ice bath when the strongest peak (dipolar plasmon peak for nanocubes) red-shifted to a desired wavelength (this red-shift is known to be size-dependent (Mahmoud et al., 2011)) and a small but distinct peak at 350 nm was visible (indicative of sharp-edged nanocube structures). The product silver nanocubes were then spun in a microcentrifuge to condense them to a smaller volume and exchange their colloidal solvent from ethylene glycol to ethanol. Washing by continued centrifugation and exchange of supernatant solution was carried out further to ensure stable and relatively monodisperse silver nanocubes in the solution.

The gold nanocages were synthesized by galvanic displacement of the previously prepared silver nanocubes (Skrabalak et al., 2008). The colloidal silver nanocubes in ethanol were exchanged to be suspended in distilled, deionized water, and then redispersed in 10 mL of a previously prepared solution of 1 mg mL^{-1} PVP in deionized water. The solution was heated to boiling in an oil bath for 10 min. A solution of 0.1 mM of tetrachloroaurate · trihydrate ($HAuCl_4 \cdot 3H_2O$) was prepared and added to the hot silver solution until the solution became deep, translucent blue in color, and a dipolar resonance above 600 nm was observed by UV–vis spectroscopy (the exact shifting of the resonance peak was dependant on the size of the starting silver nanocubes and the ratio of gold to silver remaining in the nanostructure). A typical galvanic displacement had a gold:silver ratio of 1:5, allowing for the formation of hollow structures. The resulting product of gold nanocages was then condensed and washed with water to remove excess PVP and silver chloride by-product, before exchanging and redispersing in a desirable deposition solvent.

2.3. Fabrication of the TFBG biosensors

(3-aminopropyl)trimethoxysilane (APTMS), glutaraldehyde, cysteamine, gold nanospheres (AuNS, 30 nm), 11-mercaptoundecanoic acid (MUA, 98%), N-(3-dimethylaminopropyl)-N′-ethylcarbodiimide hydrochloride (EDC), N-hydroxysuccinimide (NHS), avidin, biotin, and phosphate buffer tablets (PBS, 100 mM, pH 7.4) were purchase from Sigma-Aldrich Co. All buffer solutions were prepared using doubly deionized water from a Milli-Q water system (Thermo Fisher Scientific Inc.). After each modification of the fiber's surface, the entire array was rinsed with Milli-Q deionized water.

The effectiveness and sensitivities of the sensors containing nanoparticles were compared against the reference sensor without nanoparticles. The reference sensor consisted of only two layers of thin films. The first thin-film layer was solely APTMS (10% in water), self-assembled over 2 h in order to functionalize the outside wall of the TFBG basic sensor by silanization. The second thin-film layer was glutaraldehyde (2.5% in water), a simple and well-known amine-reactive homobifunctional crosslinker, self-assembled onto the APTMS layer over 30 min. This layer then reacted spontaneously with avidin (1 mg/mL) over 1 h, covalently bonding the avidin on the surface of the TFBG. Solutions containing different biotin concentrations were then tested on all the prepared biosensor platforms.

The fabrication of the sensors utilizing gold nanoparticles began with the same thin-films of APTMS and glutaraldehyde, as described above. The subsequent binding of the gold nanoparticles required a thiol compound, thus cysteamine was chosen for this purpose. The prepared TFBG platform was dipped into an aqueous solution of cysteamine (0.5 M) for 1 h. Finally, the TFBG platform was dipped into a solution of gold nanoparticles to covalently bind the nanoparticles (either AuNS or AuNC) to the exposed thiol sites on the fiber. In a previous study, Bialiayeu demonstrated that the sensitivity of a TFBG increased with the deposition of nanowires (Bialiayeu et al., 2012). Using those results, the deposition time of the gold nanospheres (AuNS) was set at 1 h. To achieve approximately the same initial wavelength for the two sensor platforms, the deposition time for the gold nanocages (AuNC) was 2 h. The different deposition times and particle shapes result in a red-shift of the wavelength of interest (1538 nm) by 135 pm. Then to graft the biomolecule to the TFBG, the gold-coated TFBG platform was functionalized with a self-assembled monolayer of MUA (10 mM in ethanol).The carboxyl groups of this latest monolayer were activated by a freshly prepared aqueous solution of EDC (0.2 M) and NHS (0.05 M) for 20 min. The activated sensor was finally immersed in a solution of avidin (1 mg mL^{-1}) for 1 h. The TFBG biosensor was then rinsed overnight in PBS to deactivate any remaining active groups on the surface, and finally tested with different concentrations of biotin in solution.

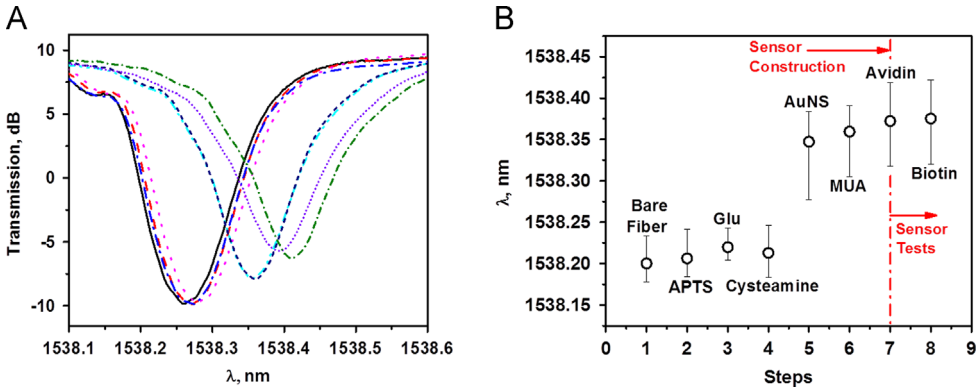

Fig. 2. (A) Shifting of the 1538 nm peak observed by transmission spectra during fabrication steps of the biosensor. With respect to the minimum of each spectra, from left to right are scans of the TFBG platform with each subsequent layer addition: bare TFBG fiber (black); addition of APTMS thin-film (red); cysteamine functionalization (dark blue); addition of glutaraldehyde layer (pink); immobilization of AuNS (light blue); functionalization of AuNS with MUA (dark purple); grafting of avidin (light purple); and after immersion in a test solution of biotin (green; 10^{-4} M). (B) The average position shifts of the cut-off wavelength during the sensor construction (by each additional layer of functionalization) and a biotin test. (For interpretation of the references to color in this figure legend, the reader is referred to the web version of this article.)

2.4. Analysis of the experimental data

A typical transmission spectrum obtained with the TFBG sensor submerged in water is presented in Fig. 1(B). The wavelength denoted by the arrow represents the cladding resonance known to be most sensitive to coupling interactions. This resonance corresponds to the last mode guided by the cladding, before the cut-off point beyond which light escapes into the outer medium. This last guided mode is the one with an evanescent field that has the maximum penetration in the outer medium while still being confined by the cladding, and hence maximum sensitivity to changes occurring on top of the cladding. The analysis presented in this paper is based on tracking the changes to this cut-off wavelength of approximately 1538 nm. Analysis of the transmission signal's changes was carried out by comparing the intensity of this peak as well as the shifting of the wavelength away from its original position. This method can be accurately applied when the change of refractive index is relatively small between trials and platform types.

2.5. Devices

The light source used in scanning the sensors was a JDS Uniphase OMNI 2 Swept Wavelength System fiber optic component analyzer, scanning from 1520 to 1620 nm. All our sensors were simply connected to this instrument via a spliced connector.

A VCA Optima system (AST products Inc.) was used for contact angle analysis in tandem with the associated software, VCA OptimaXE version 1.90.0.15. The size of droplet used in this analysis was 10uL of water.

The electron microscopes used for analysis throughout this study were a scanning electron microscope (model Tescan Vega-II XMU VPSEM) and a transmission electron microscope (model FEI Tecnai G2 F20).

3. Results and discussion

3.1. Characterization of nanoparticles

Two different geometries of gold nanoparticles were used in the fabrication of the biosensors used in this study. Ultraviolet–visible (UV–vis) spectroscopy and transmission electron microscopy (TEM) were used to observe and characterize their structure and composition parameters during and after synthesis.

The gold nanospheres obtained from Sigma-Aldrich Co. had an average diameter of 30 nm. The concentration estimated by the supplier was 1.8×10^{11} nanoparticles/mL. From the UV spectrum taken to confirm their characterization, maximum absorption was observed at 520 nm.

The size of the synthesized cubic gold nanocages was determined by analysis of obtained TEM images, being of an average edge length of 30 nm. The AuNC are hollow with porous cubic faces, allowing for functionalization inside and outside of the nanoparticle structure. This particularity of structure gives the AuNC a higher surface contact area than the AuNS. The synthesized solution of AuNC was diluted to achieve a similar intensity at maximum absorption to that of AuNS. The concentration of the AuNC was then within an order of magnitude to that of the AuNS at 1.8×10^{11} nanoparticles/mL. Similar to previous experiments (Skrabalak et al., 2008), maximum absorption observed by vis–NIR spectroscopy for the AuNC solution was 620 nm.

3.2. Fabrication of the biosensor

Transmission spectra were obtained between the additions of the functionalization layers and thin-films throughout the preparation of the TFBG biosensor. As shown in Fig. 2(A), each subsequent modification of the TFBG's surface induced a further red-shift of the cut-off wavelength near 1538 nm as well as a decrease of the peak's intensity.

Fig. 2(B) shows the position shifts of the resonance of interest in the transmission spectra, as induced by changes to be overall film thickness during the biosensor fabrication and tests. After binding the layers required to immobilize the gold nanoparticles (APTMS, glutaraldehyde, and cysteamine thin-films), the total red-shift observed was 134 pm. As the film thickness increased, the average refractive index of the cladding's local environment (comprised of the thin-film layers and water interactions) also increased. This altered the cladding-mode propagation, which in turn changed the resonance matching conditions between the incident core guided light and this cladding mode. The end result of these changes is a shift of the transmission spectrum notch associated with coupling to this particular cladding mode. Similarly, the addition of the MUA functionalization and avidin binding also produced an increase in the reflective index of the cladding environment. Upon testing the biosensor with biotin at a concentration of 10^{-4} M, a red-shift of approximately 13 pm was observable, indicative of the specific interaction between avidin and biotin.

3.3. Nanoparticles immobilization

A chemical modification of the TFBG surface enabling the covalent binding of the gold nanoparticles was incorporated into the biosensor fabrication process. This modification allowed the nanoparticle layer to be grafted into the biomolecule sensing layer. The film structure extending from the surface of the TFBG resembled a self-assembled multilayer of successive imine bonds, ending with the gold nanoparticles, as described in the schematic in Fig. 3(A).

The surface of the TFBG was first functionalized with APTMS. The silanol ends allowed a covalent binding (Kaas and Kardos, 1971) between the fiber surface and the molecule, creating a very stable chemical structure and a uniform organic layer over the TFBG by the self-assembled orientation of the long carbonyl chain of the APTMS molecule. Cysteamine was used to cap the first set of layers of the sensing film, the thiol group of which then spontaneously reacted with gold (Liu et al., 2001). Used to bind the amino groups of the APTMS layer to those of the cysteamine layer was the amine-reactive cross-linker glutaraldehyde (Habeeb and Hiramoto, 1968). This cross-linker covalently bound cysteamine to the system being fabricated and caused a reticulation of the APTMS monolayer. This reticulation shortened the distance between the base TFBG platform and the unbound solution, increasing the sensitivity of the sensing platform.

AFM imaging, seen in Fig. 3(B), showed the AuNC bound to the TFBG platform. The required absorption and binding time for each type of gold nanoparticle was determined experimentally. The criterion of completion of binding of the gold nanoparticles was to achieve a similar shift of the transmission peak of interest in a series of spectra for both types of nanoparticles. The density of the bound gold nanoparticles corresponding to the same maximal shift in the TFBG platform's spectra was determined by analysis of scanning electron microscopy (SEM) images of each respective platform, and was found to be approximately 30 particles/μm^2 for AuNC and 34 particles/μm^2 for AuNS.

3.4. Characterization of the gold nanoparticles bound to the TFBG surface

The same deposition of thin-films and nanoparticles as described previously was performed on a glass slide to enable confirmation of the desired modification and functionalization as carried out on the TFBG platform.

A contact angle goniometer was used to confirm the binding of the gold nanoparticles to the TFBG platform, as well as the functionalization by MUA of the gold nanoparticles. The contact angle of the TFBG platform without bound gold nanoparticles averaged at 60°, whereas with gold nanoparticles bound to the surface, either AuNS or AuNC, the average contact angle increased to 68°. This increase in contact angle was caused by the reaction between the free thiol ends of the cysteamine molecules and the gold nanoparticles, thus capping the TFBG surface with the hydrophobic noble metal nanostructures. When the gold nanoparticles were subsequently functionalized with MUA, the capping layer then consisted of mostly carboxylic acid groups, making it more hydrophilic, consequently decreasing the contact angle. However, for this functionalization, there was a distinct difference between the two types of gold nanoparticles. The average contact angle for MUA-capped AuNS was 58.5°, whereas that of MUA-capped AuNC was 50.5°. This was explained by the difference of specific surface contact area between the two nanoparticle shapes. AuNS are solid spheres with a specific surface area of approximately 19 nm^2 for binding MUA, while AuNC have porous faces in the cubic structure. The specific surface area for binding MUA was thus much greater as the inner and outer surface of the AuNC can be functionalized by the thiol-ended molecule. The amount of MUA molecules bound to each AuNC was significantly higher than to each AuNS, thus significantly decreasing the hydrophobicity initially caused by the gold nanoparticles at the surface of the TFBG platform. This decrease in hydrophobicity was an important factor used to increase the sensitivity of the biosensor by allowing more unbound solution to come into contact with the protein binding sites of the TFBG platform.

The TEM images, (A) in Fig. 4 display samples of the commercially available AuNS and the AuNC synthesized for this study (C). The average diameter of the AuNS, and the average side length of the AuNC was 30 nm. The functionalization of the gold nanoparticles by MUA was faintly visible by TEM imaging, as seen in Fig. 4 (B and D) as a darker halo around the nanoparticles in contrast to the imaging grid beneath the nanoparticles. The thickness of this layer was estimated to average 11.8 nm as determined by the TEM analysis software. This value was close to the expected thickness of 10 nm as found with High Resolution Electron Energy Loss Spectroscopy by Magnee et al., (2003).

3.5. Sensor parameters

Sensor performance was characterized by analysis of sensitivity, specificity and the dissociation constant, (K_d) with respect to the target biomolecule.

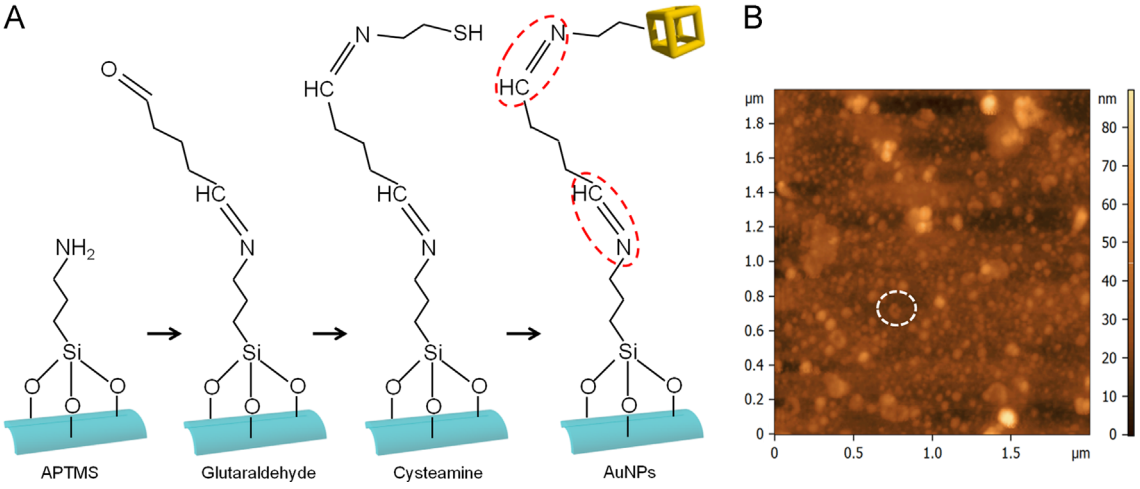

Fig. 3. (A) Schematic representation of the successive chemical additions occurring on the surface of the TFBG platform prior to the binding of gold nanoparticles; (B) atomic force microscopy (AFM) image of the fiber surface coated with AuNC. The circle indicates one of many AuNC identified clearly by parallel orientation relative to the surface of the fiber.

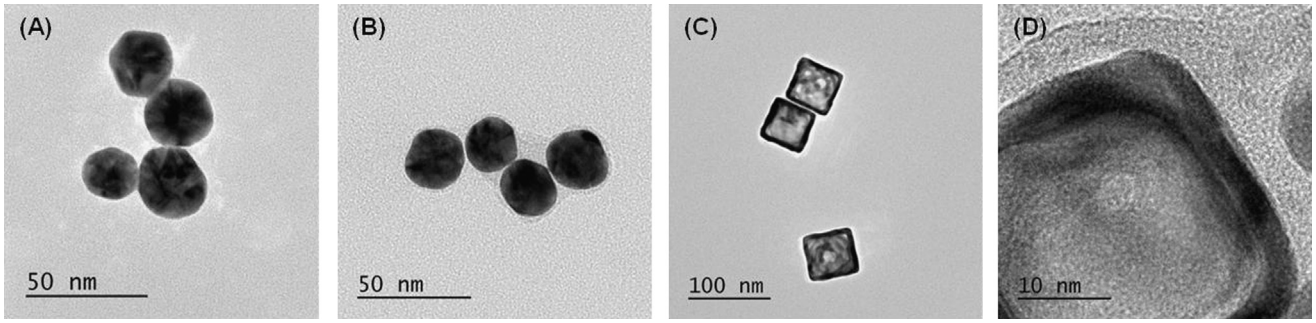

Fig. 4. TEM images of (A) bare AuNS, (B) AuNS functionalized with MUA, (C) synthesized AuNC, and (D) AuNC functionalized with MUA.

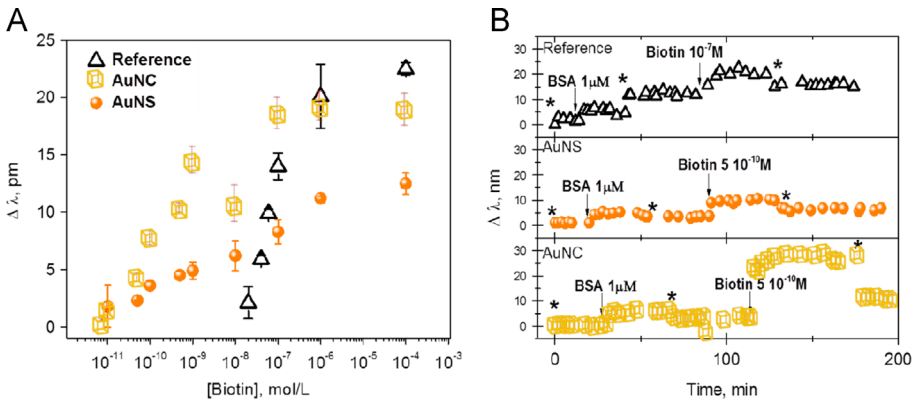

Fig. 5. (A) Responses obtained from test solutions of varying biotin concentration. (B) specificity sensorgrams obtained from each biosensing platform. (Step * corresponds to a PBS rinsing).

The first round of experiments involved exposing the TFBG sensor to solutions in a range of biotin concentrations in order to establish response curves of both types of TFBG platforms. Fig. 5 depicts the signal shift ($\Delta\lambda$), versus biotin concentration. $\Delta\lambda$ was defined as $\lambda-\lambda_0$, where λ_0 was the 1538 nm peak position measured after the functionalization with avidin and λ was the position of the same peak in the presence of biotin for each concentration of biotin tested.

The response curves observed for each biosensor platform were pseudo-first order curves demonstrating steep initial signal increases followed by regions of plateau, indicating signal saturation. The signal saturation was indicative of binding-site saturation on the biosensor. Points on the sensorgrams are separated by about 2 min, the time it takes for our system to complete a full scan. While there is evidence of biotin–avidin binding kinetics (especially for the NC case), faster sampling would be needed to fully resolve the kinetics. Faster interrogation systems exist for the measurement of fiber grating wavelength shifts (at least to kHz) rates, but there would be trade-offs to explore because higher speeds often translate into increased measurement noise. The linear increase region of the response curves were used to determine the sensitivity of the biosensor arrays. The sensitivity of the reference biosensor, constructed without gold nanoparticles was 14.96 ± 2.28 pm L mol^{-1}. The biosensor platforms constructed with AuNS and AuNC had sensitivities of 1.41 ± 0.25 pm L mol^{-1} and 5.61 ± 0.20 pm L mol^{-1} respectively. The uncertainty limits were calculated using statistics from different experiments for each case. It was clear from these results that the reference sensor had the best sensitivity. The avidin layer was bound directly to the glutaraldehyde layer in this arrangement, thus allowing the surface to be fully saturated with protein.

The evaluation of the specificity of the biosensors was carried out using an alternative protein, namely bovine serum albumin (BSA). Fig. 5(B) represents the peak shifting ($\Delta\lambda$) versus time for the detection first of BSA, then of biotin. On the reference biosensor, BSA and biotin shifted the signal by 10 pm and 3.8 pm respectively. The two proteins were thoroughly bound to the surface, as evidenced by the continuous binding activity of the glutaraldehyde layer even after rinsing the biosensor platform. This continued binding activity was caused by the nucleophilic nature of the proteins allowing for spontaneous reaction with the aldehyde group at the surface of the TFBG platform. The non-specific binding evidenced with the reference sensor also explained the apparent increase of sensitivity in that the platform is readily absorbing any protein in solution at low concentrations, not just the target protein.

By the same consideration, BSA caused a peak shift of less than 2.6 pm for both nanoparticle-containing biosensors, while $\Delta\lambda$ for the target biotin was between three to four times that of BSA. The non-specific absorption for these platforms was not influenced by the global charge of the proteins. The isoelectric points of BSA and biotin are 5 and 3.5 respectively (Ge et al., 1998; Uptima) indicating that biotin is a highly polar molecule. Moreover, at pH 7.4, the MUA monolayer and biotin have the same global charge, thus they are not attracted. Therefore, the non-specific absorption to these biosensors could be a result of the hydrophobic interactions between the proteins and the gold nanoparticles, especially considering that it is well known that proteins stick to hydrophobic surfaces including metal (Hlady and Bujis, 1996). For this reason, it is essential to maintain at least a minimum separation between the protein and the inorganic nanoparticles while minimizing interference with the biosensor's binding sites. The simplest method to achieve this minimum separation is to utilize a self-assembled monolayer (SAM) to act as a barrier on the gold nanoparticles. An MUA SAM on the gold nanoparticles reduced the amount of protein absorbed to the gold structures, though it did not completely stop protein absorption because of the hydrophobicity of MUA inherent to the grouping of the eleven-carbon chains. However, the absorption of proteins onto MUA is significantly less than that onto bare gold, thus

reducing the non-specific absorption as compared to the reference sensor, allowing the biosensors containing gold nanoparticles to better discriminate in favor of the target protein.

The limit of detection (LOD) of biotin was calculated to be the concentration that yields a signal 3 times the average noise level (Vial and Jardy, 1999). The limits of detection for the reference, AuNS, and AuNC biosensors were 9×10^{-8} mol L^{-1}, 1.1×10^{-11} mol L^{-1}, and 8×10^{-12} mol L^{-1} respectively. Comparable studies included the use of gold nanodots on an optical fiber with a LOD of 6×10^{-12} mol L^{-1} (Lin et al., 2010). Other techniques for biotin detection, including electrochemical magneto (Linares et al., 2012) and lateral flow immunoassays (Kergaravat et al., 2011), achieved a LOD on the order of 10^{-8} mol L^{-1}. The LOD obtained in this study by the use of gold nanoparticle-incorporated biosensors were at least comparable to the previously determined value by Lin et al. The gold nanoparticles had distinct LSPR, furthering the localization of light in and around the nanoparticles and led to the increase of the sensitivity of the wavelength shifts of the TFBG resonances. Since the gold nanoparticles were incorporated at the outer edge of the biosensor's thin film layers, the sensitivity to environmental changes was also increased, especially with respect to target solution concentrations. LSPR are defined as the oscillations of conduction electrons in the surface of the metallic nanoparticles. These oscillations are very strongly enhanced in the presence of electromagnetic fields, and are sensitive to changes in the local environment of the nanoparticles. The process of detection of proteins at the interface of a biosensor has been shown to be more precise when the spatial sensitivities were on the nanometer scale (Anker et al., 2008; Mayer and Hafner, 2011; Piliarik et al., 2012). Furthermore, Gao et al. (2012) demonstrated that cuboids nanoparticles created nanoscale plasmonic junctions, unique to the flat contact surface of the nanostructure, that allowed the propagation of the LSPR through all like-oriented nanocrystals within the nanostructure. This phenomenon has also been described with respect to the surface of a TFBG (Bialiayeu et al., 2012). The dependence of the nanostructure orientation on the chain length of the binding layers aided to explain the lower LOD when using AuNC than when using AuNS. The AuNC had a more distinctive and discernible orientation than the AuNS, allowing for a greater enhancement of the transmission signal when bound to the TFBG biosensor platform.

The determination of the dissociation constant (K_d) is another parameter essential to the development and comparison of efficiency of biosensors. K_d is the parameter used to characterize the binding strength between two interacting molecules, which in this case specifically applied to the target biotin interacting with avidin bound to biosensor platform.

The K_d of the biotin–avidin complex was determined by the least-squares fit of the data for the low biotin concentrations, where the concentration of biotin, was less than or equal to 5×10^{-10} mol/L according to the Langmuir absorption isotherm model (Chang et al., 2012; Li et al., 2013), as shown in Eq. (1) below.

$$[\text{biotin}]/\Delta\lambda = 1/\Delta\lambda_{max}[\text{biotin}] + K_d/\Delta\lambda_{max} \quad (1)$$

As shown in Fig. 6, the least-squares fit of the data obtained for the AuNC biosensor gave K_d for the biotin–avidin complex to be 9×10^{-14} mol L^{-1}. The same least-squares fit analysis applied to the data obtained with the AuNS biosensor gave K_d to be 7×10^{-14} mol L^{-1}. These results are close to the accepted literature value of K_d reported earlier (10^{-15} mol L^{-1}), as well as close to the K_d of transistors biosensors (Green, 1963; Li et al., 2013). These results demonstrate that TFBG coated with gold nanoparticles can be used as a biosensing platform for the detection of biomolecule targets at small concentrations allowing for the development of a series of portable biosensors that can be applied in situ for the measurement of biomolecular interactions without perturbing the surrounding environment.

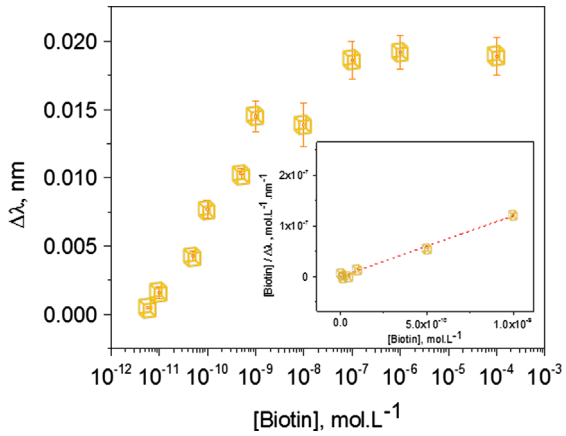

Fig. 6. Shifting of the 1538 nm peak with respect to biotin concentration for the AuNC biosensor. The inset shows the least-squares fit (Eq. (1)) of the measured ratio of concentration of biotin to wavelength shift as a function of concentration of biotin.

4. Conclusion

This study demonstrated how a TFBG sensor, used in reflection mode with a single-mode fiber, can be applied as a biosensor to detect biomolecules. The results indicated that the TFBG can be used as an optical transducer for making biosensors and constitutes an inexpensive alternative to biosensing platforms currently being employed. Specifically, this study showed that the system can be easily modified with chemical and nanostructured thin-films, and can be used for in situ measurements. The simple methods of modification can also be monitored continuously throughout the addition of each functionalization layer, including through the binding of biotin to avidin grafted onto the surface of the TFBG platform. By having a functional sensor throughout the fabrication process, the quality of the surface functionalization can be assessed prior to using the sensor for the target application (and "bad" sensors sorted out). Binding gold nanoparticles to the surface of the TFBG biosensor provided a strong signal for the detection of biotin in a phosphate buffer solution. The gold nanoparticles were used as a magnification layer to enhance the light localization in and around the nanoparticles, thus enhancing the peak shifts in the transmission spectra. The AuNC were found to induce a lower LOD and sensitivity than the AuNS in the biosensor, likely due to their increased contact area (for a similar overall size). The LOD of the TFBG biosensor associated with gold nanoparticles was three orders of magnitude greater than that of the reference biosensor, demonstrating that this sensor platform is a powerful yet sensitive biosensor.

References

Albert, J., Shao, L.Y., Caucheteur, C., 2013. Laser and Photonics Reviews 7 (1), 83–108.
Anker, J.N., Hall, W.P., Lyandres, O., Shah, N.C., Zhao, J., Van Duyne, R.P., 2008. Nature Materials 7 (6), 442–453.
Bedford, E.E., Spadavecchia, J., Pradier, C.M., Gu, F.X., 2012. Macromolecular Bioscience 12 (6), 724–739.
Bernand-Mantel, D., Chehimi, M.M., Millot, M.C., Carbonnier, B., 2010. Surface and Interface Analysis 42 (6–7), 1035–1040.
Bialiayeu, A., Bottomley, A., Prezgot, D., Ianoul, A., Albert, J., 2012. Nanotechnology 23, 44.
Bialiayeu, A., Caucheteur, C., Ahamad, N., Ianoul, A., Albert, J., 2011. Optics Express 19 (20), 18742–18753.

Bousalem, S., Benabderrahmane, S., Sang, Y.Y.C., Mangeney, C., Chehimi, M.M., 2005. Journal of Materials Chemistry 15 (30), 3109–3116.
Chan, C.F., Chen, G., Jafari, A., Laronche, A., Thomson, D.J., Albert, J., 2007. Applied Optics 46 (7), 1142–1149.
Chang, K.S., Sun, C.J., Chiang, P.L., Chou, A.C., Lin, M.C., Liang, C., Hung, H.H., Yeh, Y. H., Chen, C.D., Pan, C.Y., Chen, Y.T., 2012. Biosensors and Bioelectronics 31 (1), 137–143.
Corning, 2010. ⟨http://www.corning.com/opticalfiber/products/SMF-28_ULL_fiber.aspx⟩.
Fang, Z., Zhu, X., 2013. Advanced Materials 25 (28), 3840–3856.
Fu, C., Hu, C., Liu, Y., Xu, S., Xu, W., 2013. Analytical Methods 4 (10), 3107–3110.
Gao, B., Arya, G., Tao, A.R., 2012. Nature Nanotechnology 7 (7), 433–437.
Ge, S., Kojio, K., Takahara, A., Kajiyama, T., 1998. Journal of Biomaterials Science, Polymer Edition 9 (2), 131–150.
Gehan, H., Fillaud, L., Chehimi, M.M., Aubard, J., Hohenau, A., Felidj, N., Mangeney, C., 2010. ACS Nano 4 (11), 6491–6500.
Gosecka, M., Griffete, N., Mangeney, C., Chehimi, M.M., Slomkowski, S., Basinska, T., 2011. Colloid and Polymer Science 289 (13), 1511–1518.
Green, N.M., 1963. Biochemical Journal 89 (3), 585–591.
Habeeb, A.F.S.A., Hiramoto, R., 1968. Archives of Biochemistry and Biophysics 126 (1), 16–26.
Hayashida, M., Yamaguchi, A., Misawa, H., 2005. Japanese Journal of Applied Physics 44 (50–52), L1544–L1546.
Hlady, V., Bujis, J., 1996. Current Opinion in Biotechnology 7 (1), 72–77.
Hrapovic, S., Liu, Y.L., Enright, G., Bensebaa, F., Luong, J.H.T., 2003. Langmuir 19 (9), 3958–3965.
Kaas, R.L., Kardos, J.L., 1971. Polymer Engineering and Science 11 (1), 11–18.
Kaewsaneha, C., Tangboriboonrat, P., Polpanich, D., Eissa, M., Elaissari, A., 2013. ACS Applied Materials and Interfaces 5 (6), 1857–1869.
Kergaravat, S.V., Gómez, G.A., Fabiano, S.N., Laube Chàvez, T.I., Pividori, M.I., Hernàndez, S.R., 2011. Talanta 97 (0), 484–490.
Kwon, M.J., Lee, J., Wark, A.W., Lee, H.J., 2012. Analytical Chemistry 84 (3), 1702–1707.
Li, B.R., Chen, C.W., Yang, W.L., Lin, T.Y., Pan, C.Y., Chen, Y.T., 2013. Biosensors and Bioelectronics 45, 252–259.
Lin, S.P., Pan, C.Y., Tseng, K.C., Lin, M.C., Chen, C.D., Tsai, C.C., Yu, S.H., Sun, Y.C., Lin, T.W., Chen, Y.T., 2009. Nano Today 4 (3), 235–243.
Lin, Y., Zou, Y., Mo, Y., Guo, J., Lindquist, R.G., 2010. Sensors 10 (10), 9397–9406.
Linares, E.M., Kubota, L.T., Michaelis, J., Thalhammer, S., 2012. Journal of Immunological Methods 375 (1–2), 264–270.
Liu, Y.C., Wang, C.M., Hsiung, K.P., 2001. Analytical Biochemistry 299 (2), 130–135.
Magnee, R., Maazouz, M., Doneux, C., Bodino, F., Rudolf, P., Teillet-Billy, D., Pireaux, J.J., 2003. Journal of Physical Chemistry B 107 (19), 4567–4572.
Maguis, S., Laffont, G., Ferdinand, P., Carbonnier, B., Kham, K., Mekhalif, T., Millot, M.C., 2008. Optics Express 16 (23), 19049–19062.
Mahmoud, M.A., Qian, W., El-Sayed, M.A., 2011. Nano Letters 11 (8), 3285–3289.
Mayer, K.M., Hafner, J.H., 2011. Chemical Reviews 111 (6), 3828–3857.
Nguyen, T.H., Hardwick, S.A., Sun, T., Grattan, K.T.V., 2012. IEEE Sensors Journal 12 (1), 255–260.
Patolsky, F., Zheng, G., Lieber, C.M., 2006. Nature Protocols 1 (4), 1711–1724.
Piliarik, M., Šípová, H., Kvasnička, P., Galler, N., Krenn, J.R., Homola, J., 2012. Optics Express 20 (1), 672–680.
Rozenberg, B.A., Tenne, R., 2008. Progress in Polymer Science 33 (1), 40–112.
Sendroiu, I.E., Warner, M.E., Corn, R.M., 2009. Langmuir 25 (19), 11282–11284.
Shao, L.-Y., Coyle, J.P., Barry, S.T., Albert, J., 2011. Optical Materials Express 1 (2), 128–137.
Shevchenko, Y., Francis, T.J., Blair, D.A.D., Walsh, R., DeRosa, M.A., Albert, J., 2011. Analytical Biochemistry 83, 7027–7034.
Sim, H.R., Wark, A.W., Lee, H.J., 2010. Analyst 135 (10), 2528–2532.
Skrabalak, S.E., Chen, J.Y., Sun, Y.G., Lu, X.M., Au, L., Cobley, C.M., Xia, Y.N., 2008. Accounts of Chemical Research 41 (12), 1587–1595.
Spitalsky, Z., Tasis, D., Papagelis, K., Galiotis, C., 2010. Progress in Polymer Science 35 (3), 357–401.
Uptima, I., ⟨www.interchim.fr/ft/1/10685A.pdf⟩.
Vial, J., Jardy, A., 1999. Analytical Chemistry 71 (14), 2672–2677.
Yu, C., Irudayaraj, J., 2007. Biophysical Journal 93 (10), 3684–3692.
Zhou, W., Mandia, D.J., Griffiths, M.B.E., Bialiayeu, A., Zhang, Y., Gordon, P.G., Barry, S.T., Albert, J., 2013. Optics Express 21 (1), 245–255.
Zou, H., Wu, S., Shen, J., 2008. Chemical Reviews 108 (9), 3893–3957.